ADVANCED MATERIALS
www.advmat.de

Materials Views
www.MaterialsViews.com

Photo–Roll Lithography (PRL) for Continuous and Scalable Patterning with Application in Flexible Electronics

*Jong G. Ok, Moon Kyu Kwak, Chad M. Huard, Hong Seok Youn, and L. Jay Guo**

For decades, photolithography has been the industry workhorse for various micro/nanoscale fabrications because of its well-established procedure and highly reproducible results.[1] Despite steady progress in unconventional micro/nanofabrication and patterning techniques in recent years,[2] photolithography has remained the dominant technology due to its excellent reliability and globally disseminated infrastructure, along with its mature protocol of pre- and postlithography steps such as mask-making, etching, etc. On the other hand, there has been increasing interest in recent years in large-area electronic[3] and photonic applications,[4] especially for materials made on flexible substrates, where traditional photolithography has not played an important role. Instead, other continuous and scalable techniques, most notably represented by roll-to-roll (R2R) nanoimprint lithography (NIL), are flourishing for large-area and flexible pattern fabrications.[5] However, such methods involve mechanical contacts and indentation between the mask and the polymer resist, and the subsequent demolding process is prone to defect generation. Additionally, the implementation of alignment in the multiple steps of the NIL process is challenging; on the other hand, alignment and registration techniques in optical lithography are commonly used. Therefore, to meet the demands of scalability and throughput for flexible electronics, it is time to revitalize the photolithography technique toward large-area continuous patterning with significantly improved process throughput and reduced manufacturing costs. An encouraging development was recently made by extending traditional phase-shift mask photolithography[6] into a continuous process by utilizing a roll-type phase-shift mask for large-area patterning while maintaining deep submicron resolution.[7]

Dr. J. G. Ok,[+] Dr. M. K. Kwak,[+] C. M. Huard, Dr. H. S. Youn, Prof. L. J. Guo
Department of Electrical Engineering and Computer Science
University of Michigan
Ann Arbor, Michigan 48109, USA
E-mail: guo@umich.edu
Dr. J. G. Ok, Prof. L. J. Guo
Department of Mechanical Engineering
University of Michigan
Ann Arbor, Michigan 48109, USA
Prof. M. K. Kwak
School of Mechanical Engineering
Kyungpook National University
Daegu 702–701, South Korea
[+]These authors contributed equally to this study.

DOI: 10.1002/adma.201303514

Herein, we introduce a new and general methodology termed photo–roll lithography (PRL), for continuous and scalable lithographic patterning. This process integrates two outstanding characteristics of micro/nano-fabrication technology: photolithography with high reproducibility and faithful patterning, and rollable processing that is easily scalable to continuous large-area fabrication, into a versatile technique applicable to both rigid and flexible substrates. The PRL system utilizes a flexible photomask and a rollable UV exposure unit to realize the continuous photolithographic patterning of arbitrary micro/nanoscale features on a moving substrate with high throughput. The nature of the contact lithography in PRL ensures high-resolution patterning. Since PRL uses a flexible, soft mask without the aid of great force or heating, it can afford patterning on fragile substrates such as graphene layers. Based on the nature of the dynamic rolling in PRL, geometric modulation of outcome patterns is possible by using a single mask, simply by controlling the rotation speed of a mask-attached roll with respect to the substrate-feed speed. After introducing the principle and setup for PRL, we will show the single-mask fabrication of band-tunable IR filters using this feature. The versatile PRL process can be applied to various flexible electronics and photonics. We will demonstrate the continuous fabrication of transparent metal electrodes (TMEs)[8] in the form of metallic mesh as well as enhanced TMEs made by patterning metal mesh directly onto a graphene layer by using PRL. We make further use of PRL-fabricated TMEs to create polymer light-emitting diodes (PLEDs) and show the excellent flexibility of these devices.

Figure 1a depicts the main components in a PRL system: a flexible photomask, a rollable UV exposure unit, and a photoresist developing module. The flexible photomask containing the desired pattern openings is first fabricated on a 50 nm-thick Al-coated polyethylene terephthalate (PET) sheet (see Experimental Section for detailed procedure). This flexible Al/PET photomask is then conformally adhered to the outer surface of a hollow quartz cylinder using an intermediate thin polydimethylsiloxane (PDMS) layer. Inside this quartz cylinder, a 365 nm-wavelength UV light source is mounted and collimated to a 1 mm-wide aperture. A photoresist-coated substrate is then fed by a linear stage to the UV exposure roll where the contact line between the substrate surface and the roll is aligned to the UV-exposing aperture slit. The mask–substrate contact can be adjusted from contact mode to proximity mode; in the case of the contact mode, either rolling or linear feeding can drive the isokinetic mask–substrate movement by friction, while the proximity mode allows separate controls of the mask and the substrate for geometrical tuning, as will be shown later. The rolling proceeds at a speed of up to 5 mm s^{-1} with our current UV light source, although this speed can be increased by using more

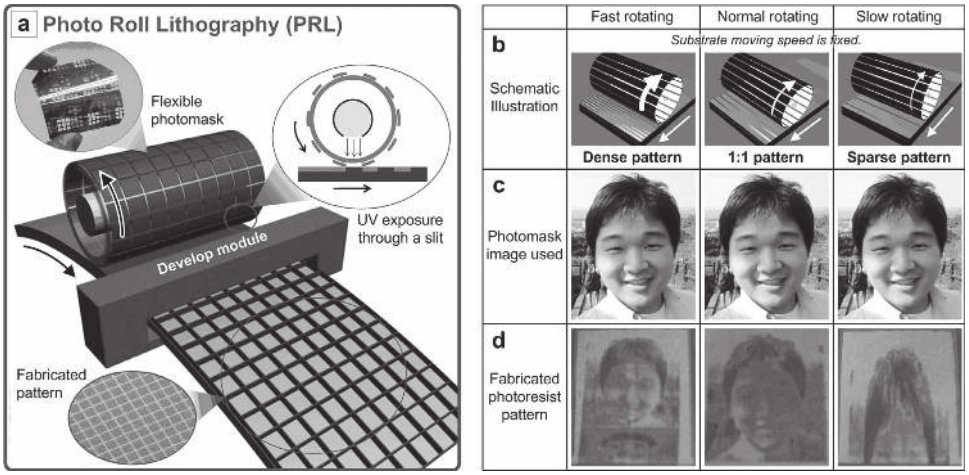

Figure 1. a) Schematic description of the PRL process; a flexible photomask (as shown in the upper left inset) is adhered to the hollow quartz cylinder inside which a collimated UV light source is mounted (as shown in the upper right inset). As the rolling proceeds, a photoresist-coated substrate continuously undergoes UV exposure and developing steps, finalizing to the desired pattern (as shown in the lower left inset). b–d) Demonstration of geometry-programmable PRL. b) Conceptual schematics illustrating that the period of line patterns can be real-time controlled in PRL by modulating the mask rotation speed with respect to the substrate movement speed. Using an identical mask to that shown in part c, more complicated patterns can also be processed to give different shapes as displayed in part d by mask–substrate motion control.

powerful UV light. As the UV light is exposed through the slit on the passing substrate, latent images of the mask patterns are formed continuously in the photoresist layer, which are finalized after the exposed resist goes through the development process.

Beyond the continuous and high-speed processability, PRL can realize real-time tuning of the pattern geometry, which enables fabrication of diverse structures out of a single mask. Whereas conventional lithography relies on the static and planar alignment of the mask and the substrate, the rolling principle of PRL allows dynamic control of the mask rotation speed with respect to the substrate feed speed during UV exposure. Here, the rollable mask and the feeding substrate are slightly separated to allow independent motion (i.e., proximity-mode printing). Depending on the relative mask–substrate motion, the shape of the resulting photolithography patterns can be modulated as illustrated in Figure 1b. Using line patterns as an example, when the mask is rolling faster than the substrate is moving, the resulting line pattern becomes denser than that on the original mask pattern, and vice versa. For more complicated patterns, the final geometry can be readily tuned to achieve different aspect ratios by using a single mask, as exhibited in Figures 1c and 1d by using a photoimage mask. Fast rotation of the roll mask compresses the original image in the substrate moving direction, while lower speed rotation elongates the image.

Since the UV exposure time may vary depending on the roller-mask rotation speed in this geometry-tunable PRL process, the UV intensity should be regulated accordingly for consistent and reliable exposure. Namely, the slow rotating speed leads to a relatively long exposure time for each opening in the photomask under constant light intensity, which can broaden or even wipe out the photoresist pattern due to overexposure. Conversely, a fast rotating speed can cause underexposure with an exposure insufficient to develop the photoresist pattern. To prevent these potential issues, the effective UV intensity (I') can be adjusted to maintain the constant dose level according to the following relationship:

$$I' = I \times (v/wr) \quad (1)$$

where I is the UV intensity calibrated for the normal contact-mode PRL process (i.e., giving the 1:1 ratio pattern), and ω, r, and v are the rotating speed of a mask roll, its radius, and the substrate movement speed, respectively.

By taking advantage of the geometry-tunable patterning in PRL, we show that a single photomask can produce manifold micro/nanostructures of varied dimensions. As a specific example, we demonstrate plasmonic IR filters with tunable absorption bands based on a metal–insulator–metal (MIM) stack[9] (i.e., Al–SiO_2–Al in our design). Here PRL is applied to continuously pattern the top metal layer into subwavelength-sized dot array to form a plasmonic MIM array and produce resonance absorptions in the IR range, similar to what has been previously investigated by utilizing the R2R NIL process.[4] While NIL produces a pattern identical to that on the mold, PRL can change the dot-pattern shape simply by real-time control of the mask–substrate motion with the original mask, thereby tailoring the desired plasmonic performance and the IR absorption bands. **Figure 2** displays flexible IR filters in which the mask rotation speed was modulated alongside a fixed substrate-feed rate to make two different patterns (Figures 2a and 2b) by using an identical photomask containing a subwavelength-scale dot pattern. The reflection Fourier-transform infrared (FTIR) spectra disclose the differences in resonance positions and polarization characteristics depending on the pattern geometry (Figures 2c and 2d); in the case of a round dot pattern (Figure 2a), the resonances are not significantly dependent on the polarization of incident IR light due to the symmetric dot shapes (Figure 2c).[4] On the other hand, the asymmetric oval dot pattern produced by faster rotation of the rollable photomask during PRL (Figure 2b) reveals stronger polarization dependence, while the resonances are blue-shifted because of the shrunken pattern size (Figure 2d). These results are preliminary, yet they suggest a clear prospective way to

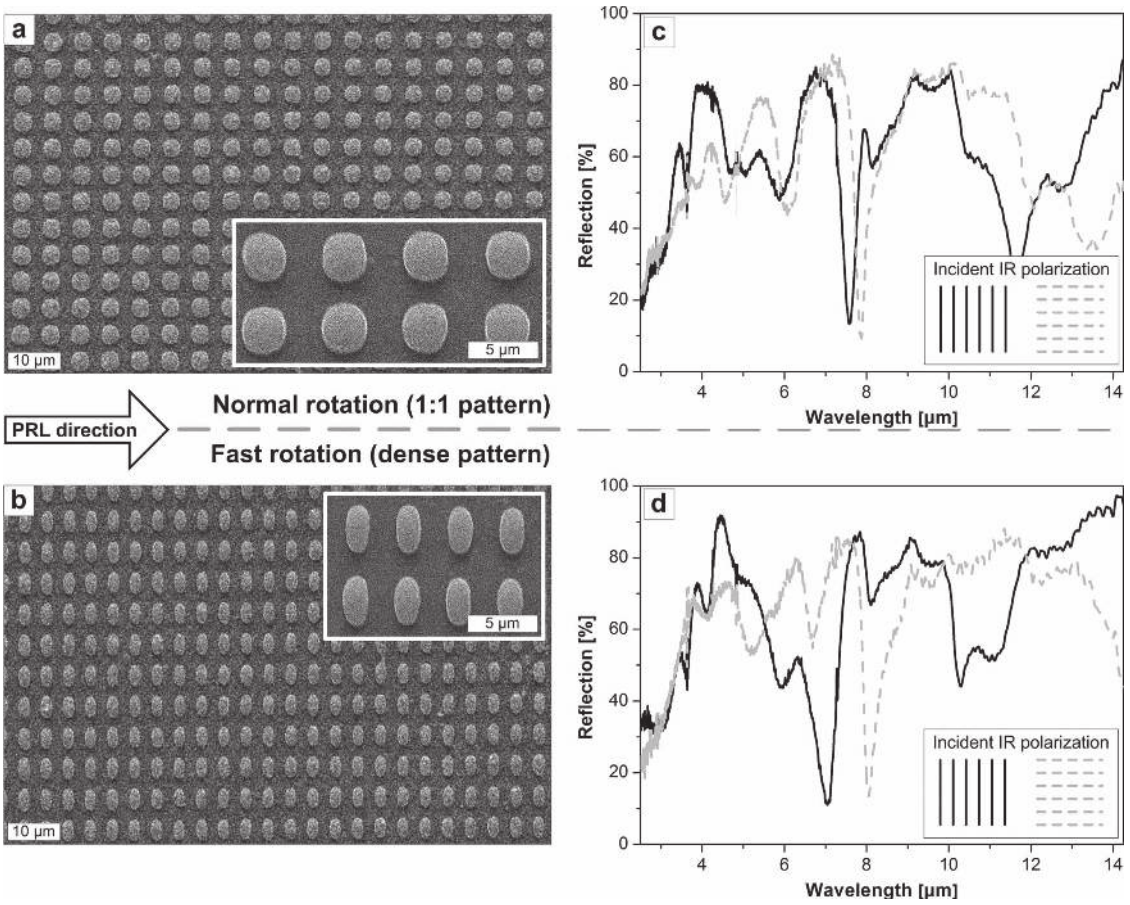

Figure 2. Single-mask fabrication of tunable plasmonic IR filters: scanning electron microscopy (SEM) images of a) round and b) oval Al dot arrays patterned on an MIM substrate by PRL using the same photomask at different mask rotating speeds. Insets to parts a and b clearly disclose that the shape and interspacing of the round dot array, obtained by moving the mask and substrate in 1:1 ratio, become smaller with faster rotation of the mask. The IR reflection spectra of c) round and d) oval dot arrays demonstrate the tunability of dip positions and polarization characteristics in the two IR filters.

tailor the desired characteristics in many micro/nanostructured devices by utilizing the PRL process to give real-time tunable patterning.

To develop tangible electronic applications by utilizing the PRL process, we now demonstrate the continuous fabrication of transparent metal electrodes (TMEs). TMEs based on an invisible metallic pattern were introduced several years ago as an alternative transparent conductor to the commonly used indium–tin oxide (ITO) for optoelectronic applications.[10] However a truly scalable manufacturing process, especially for flexible electronics, is still lacking. Here we describe TMEs made by fabricating a metal mesh pattern on either flexible (e.g., PET) or rigid (e.g., glass) transparent substrates in a continuous fashion. After the flexible photomask containing designed mesh patterns has been prepared and attached to the roll, PRL is performed in contact mode over the photoresist-coated transparent substrates, which have either a metal layer or a metal/graphene layer, followed by resist development and wet-etching processes.

We first systematically investigate the Al mesh patterns made by PRL by parameterizing the Al thickness as well as the mesh cell size, then demonstrate the PRL processing of Al mesh patterns on a graphene layer to further improve the perfomance of TMEs for a broader range of applications. **Figure 3**a shows the SEM images of the fabricated Al mesh patterns with cell sizes varying from 10–70 μm. The inset to Figure 3a zooms into the point of intersection of Al lines with 1 μm linewidth. The sheet resistances of the fabricated TME samples of each cell size with varying metal thicknesses of 20, 30, and 50 nm were measured and are plotted with the theoretically calculated values in Figure 3b. The measurements and calculations show a good agreement within 10% deviation, which indicates the faithful patterning of the PRL process. A slight mismatch between the measured and calculated values might result from defects (e.g., metal line disconnections) and/or the natural oxidation of Al. Figure 3c shows the optical transmittance of the TME samples fabricated on glass substrates, with bare glass as a reference. To avoid complexity and show the trend more clearly, we collected transmittance values for each sample at 550 nm wavelength from the complete visible spectra with wavelengths covering 400–800 nm. As exemplified by the 30-μm cell data in the inset to Figure 3c, the transmittance values appear almost constant over the entire visible wavelength range, which is highly desirable in most applications.

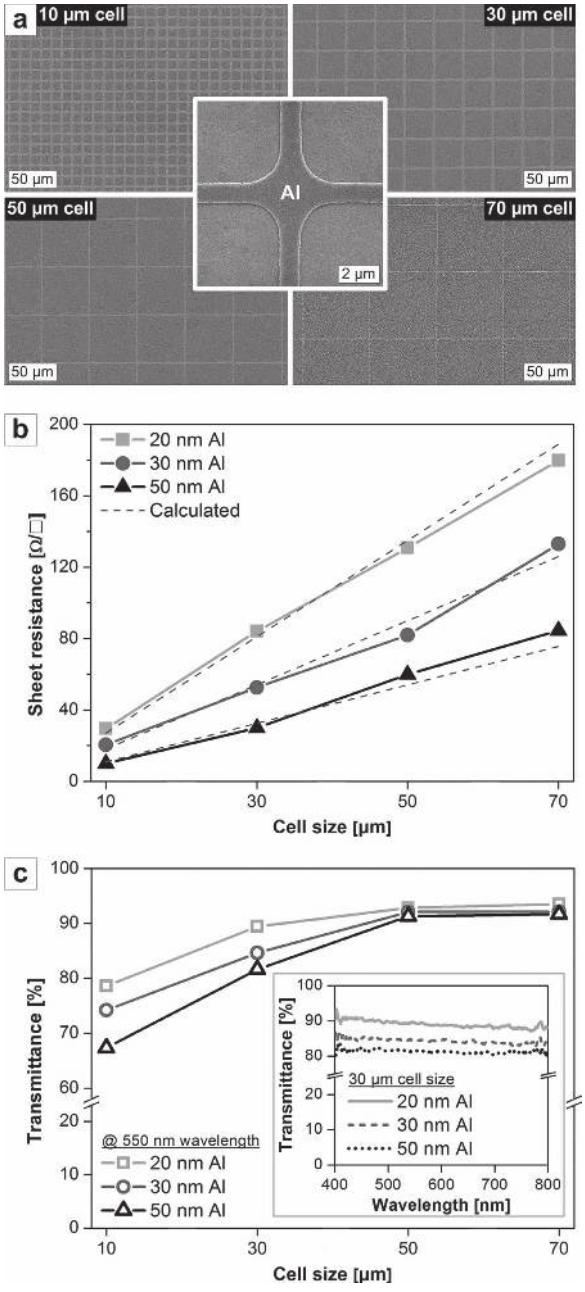

Figure 3. Application of PRL in TME fabrication: a) SEM images of the PRL-fabricated Al mesh-based TMEs with varying mesh cell sizes. The inset reveals the clearly defined Al line patterns with 1-μm linewidth. b) Sheet resistances and c) transmittances at 550 nm of the TMEs fabricated with different period and Al thickness. Dashed lines in part b indicate theoretically calculated values. The transmittances of the 30 μm period samples along the entire visible range are shown in an inset to part c.

There is a trade-off between the sheet resistance and the transmittance of the fabricated TMEs; the transmittance increases with decreasing Al thickness or increasing cell size, both of which can cause an increase in sheet resistance. Nevertheless, the dependence of the transmittance on Al thickness becomes very small as the cell size increases (i.e., at 50 and 70 μm) because the areal coverage of the transparent opening becomes more dominant. The trade-off between sheet resistance and transmittance is therefore optimized at a mesh cell size of 50 μm in our study. Certainly the cell geometry is not limited to square, but can also be other shapes such as hexagon, which can be patterned easily with PRL. One can further tailor the desired TME specification by choosing the proper metal thickness and the cell size, both of which are readily achievable in PRL.

Now we demonstrate that the gentle nature of the PRL process allows direct patterning onto transferred graphene layers. While the TME fabricated by PRL has suitable resistance and transparency for touch panel applications, the spacing between the metal lines is too large for it to be used directly in other optoelectronic devices such as organic LEDs (OLEDs) or organic photovoltaics (OPVs), where charge injection or collection occurs uniformly across the transparent electrode. This problem can be solved by adding a highly conductive layer to form a composite electrode structure.[11,12] Another strategy is to incorporate a graphene layer to distribute the current. Because it has excellent electrical properties and high optical transparency,[13] a single- or few-layer graphene film transferred onto the transparent substrate can directly serve as transparent conducting electrodes.[14] However the sheet resistance of the graphene film itself is often too large for OLEDs and OPVs. The overall conductivity can be improved with little decrease in transmittance when the graphene layer is incorporated into metal grid patterns.[15] However, it could be challenging to conformally cover the graphene layer over the metal patterns on a large scale without damaging or leaving residual stress on the graphene.

We fabricate the metal mesh patterns directly on top of graphene by using PRL. Since in PRL a flexible photomask cushioned by a PDMS pad makes a soft contact on the substrate and patterning proceeds without much force, a flat graphene layer covered by a thin metal layer can remain intact throughout the PRL patterning. **Figure 4**a depicts the overall fabrication procedure of graphene-incorporated TMEs (G-TMEs). We used single- or multilayer graphene and varied the metal thickness and mesh dimension depending on the targeted function. Either glass or PET film was used as a transparent substrate; Figure 4b shows the graphene film transferred to PET. After the Al deposition on the graphene-transferred substrate, PRL was conducted to define the metal mesh pattern on top of graphene, as demonstrated in Figure 4c. The enlarged view (Figure 4d) shows that the metal pattern is cleanly formed with few defects, which is widely attributed to the gentle nature and reliability of the PRL process.

In our G-TME fabrication, we used two combinations of graphene and metal mesh pattern: 1) multilayer graphene + dense and thick metal mesh (50-μm cell size, 50-nm thick Al), and 2) single-layer graphene + coarse and thin metal meshes (150- and 750-μm cell size, 25-nm thick Al). To ensure better adhesion of the patterned Al on graphene, the mesh linewidths were designed to be 5 μm, except the 750-μm cell size mesh which had a 12-μm linewidth. Figures 4e and 4f compare the transmittance values over the visible range for the bare graphene, bare metal mesh (TMEs), and graphene–mesh combined samples (G-TMEs), and the measured sheet resistances along with

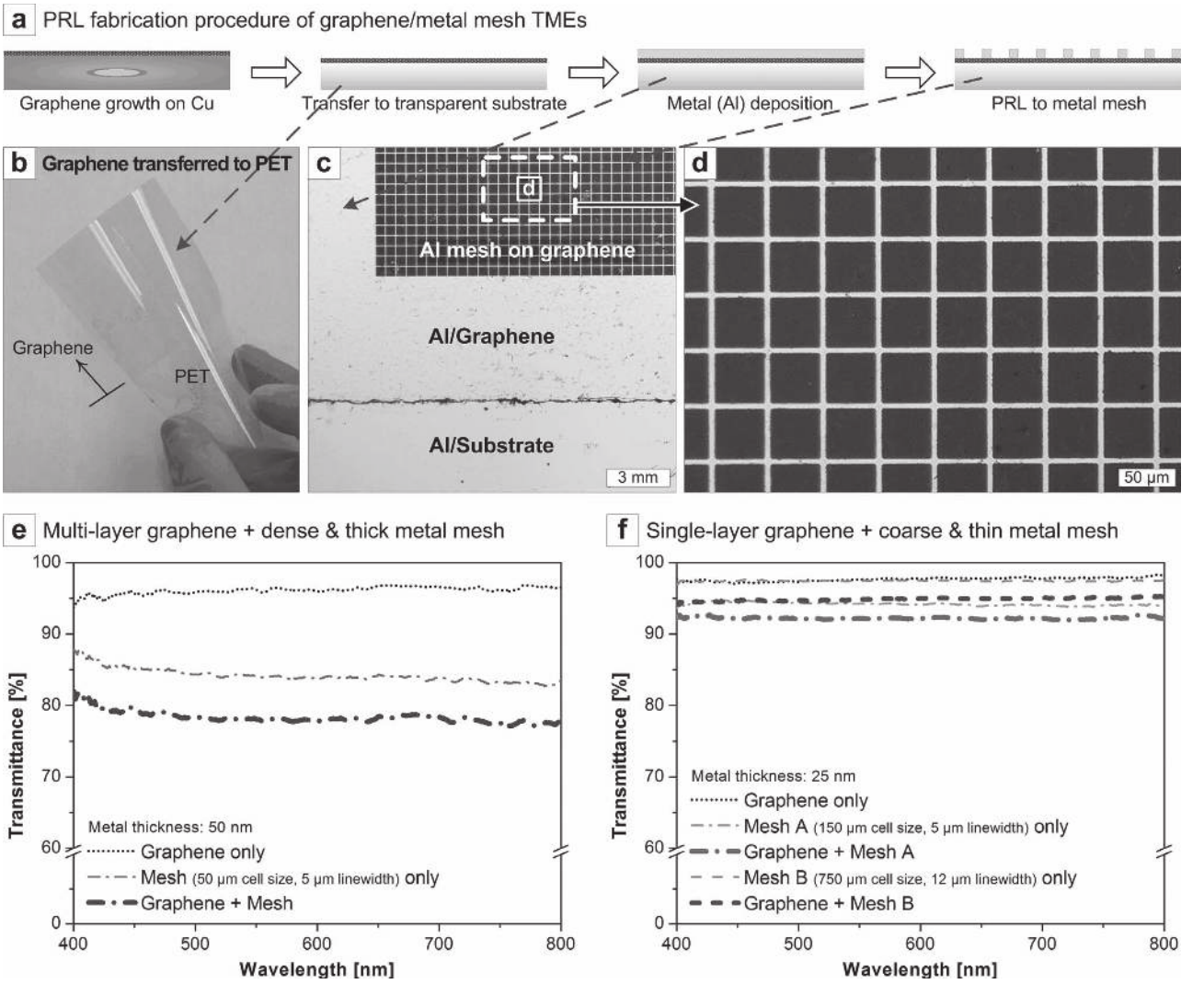

Figure 4. Incorporation of graphene to PRL for improved TME fabrication: a) Schematic illustration of overall G-TME fabrication procedure. b) Photo of graphene-transferred transparent PET substrate. c) Microscope image of the PRL-patterned Al mesh on a graphene/PET substrate. d) Enlarged view reveals cleanly defined Al mesh pattern. e,f) Optical transmittance plots indicate the transmittance values of bare graphene, bare metal mesh, and graphene-incorporated metal mesh samples for different mesh geometry and metal thickness.

representative transmittances at 550 nm wavelength of all cases are summarized in **Table 1**. Compared to bare graphene, the sheet resistance drastically decreased (i.e., 79%–97%) with much smaller decrease in transmittance (i.e., 2.9%–18%) after metal mesh patterning on graphene by PRL. Interestingly, the total combined resistance (R_{tot}) and transmittance (T_{tot}) values of G-TMEs can be predicted from those of graphene (T_g, R_g) and metal mesh (T_m, R_m) based on the following equations:

$$R_{tot} = \left(R_g^{-1} + R_m^{-1}\right)^{-1} = \left(R_g \times R_m\right)/\left(R_g + R_m\right) \quad (2)$$

$$T_{tot} = 1 - \left((1 - T_g) + (1 - T_m)\right) = T_g + T_m - 1 \quad (3)$$

where Equation (2) simply means that the metal mesh layer and the graphene layer are electrically connected in parallel, and Equation (3) assumes that transmittance is purely determined by the absorption of each layer. Here the scattering effect is small and neglected. The calculated values are well-matched to the measurement data as indicated in Table 1, which confirms that the metal mesh can be successfully patterned on the graphene film by PRL with few defects and negligible degradation of electrical property of either metal mesh or graphene.

To show the utility of the G-TME for flexible-electronic-device application, we use it as flexible and transparent electrode for PLEDs. The device structure is illustrated in **Figure 5**a, where a (G-)TME serves as an anode and super yellow (SY, yellow light-emitting polymer) is used as an emissive layer. Fabrication details and functions of each layer are described elsewhere.[16] To ensure conformal coating of thin active layers over (G-)TMEs without short circuit, we chose Al layers as thin as 25 nm. Since graphene can function as an OLED anode by itself,[17] we chose a coarse mesh pattern (i.e., 750-μm cell size, 12 μm linewidth) to investigate how graphene affects metal mesh TMEs in LED operation.

Table 1. Measured sheet resistances of graphene, bare TMEs, and G-TMEs for different metal mesh geometry and thickness, and their comparison to calculated values.

Graphene type/mesh specification (cell size [μm] / Al thickness [nm])		Graphene	Mesh (TMEs)	Graphene + mesh (G-TMEs)
Multilayer graphene + dense and thick mesh (50/50)	Sheet resistance [Ω □$^{-1}$] (decrease % from graphene)	469.8	14.3	14.0 (97%)
	Calculated combined resistance [Ω □$^{-1}$] (Equation (2))			13.8
	Transmittance [%] at 550 nm wavelength (decrease % from graphene)	95.2	84.1	78.0 (18%)
	Calculated combined transmittance [%] (Equation (3))			79.4
Single-layer graphene + coarse and thin mesh (150/25)	Sheet resistance [Ω □$^{-1}$] (decrease % from graphene)	1208	131.9	118.8 (90%)
	Calculated combined resistance [Ω □$^{-1}$] (Equation (2))			118.9
	Transmittance [%] at 550 nm wavelength (decrease % from graphene)	97.6	94.2	92.1 (5.6%)
	Calculated combined transmittance [%] (Equation (3))			91.8
Single-layer graphene + coarse and thin mesh (750/25)	Sheet resistance [Ω □$^{-1}$] (decrease % from graphene)	1208	287.7	248.8 (79%)
	Calculated combined resistance [Ω □$^{-1}$] (Equation (2))			232.4
	Transmittance [%] at 550 nm wavelength (decrease % from graphene)	97.6	97.4	94.8 (2.9%)
	Calculated combined transmittance [%] (Equation (3))			95.0

Figure 5b comparatively displays the luminance images of PLED devices based on (G-)TME and ITO on PET substrates. The G-TME PLED device shows stable operation under bending with a radius of curvature as small as about 5 mm, while the ITO-based PLED failed upon slight bending due to cracking in the brittle ITO, which demonstrates excellent flexibility of

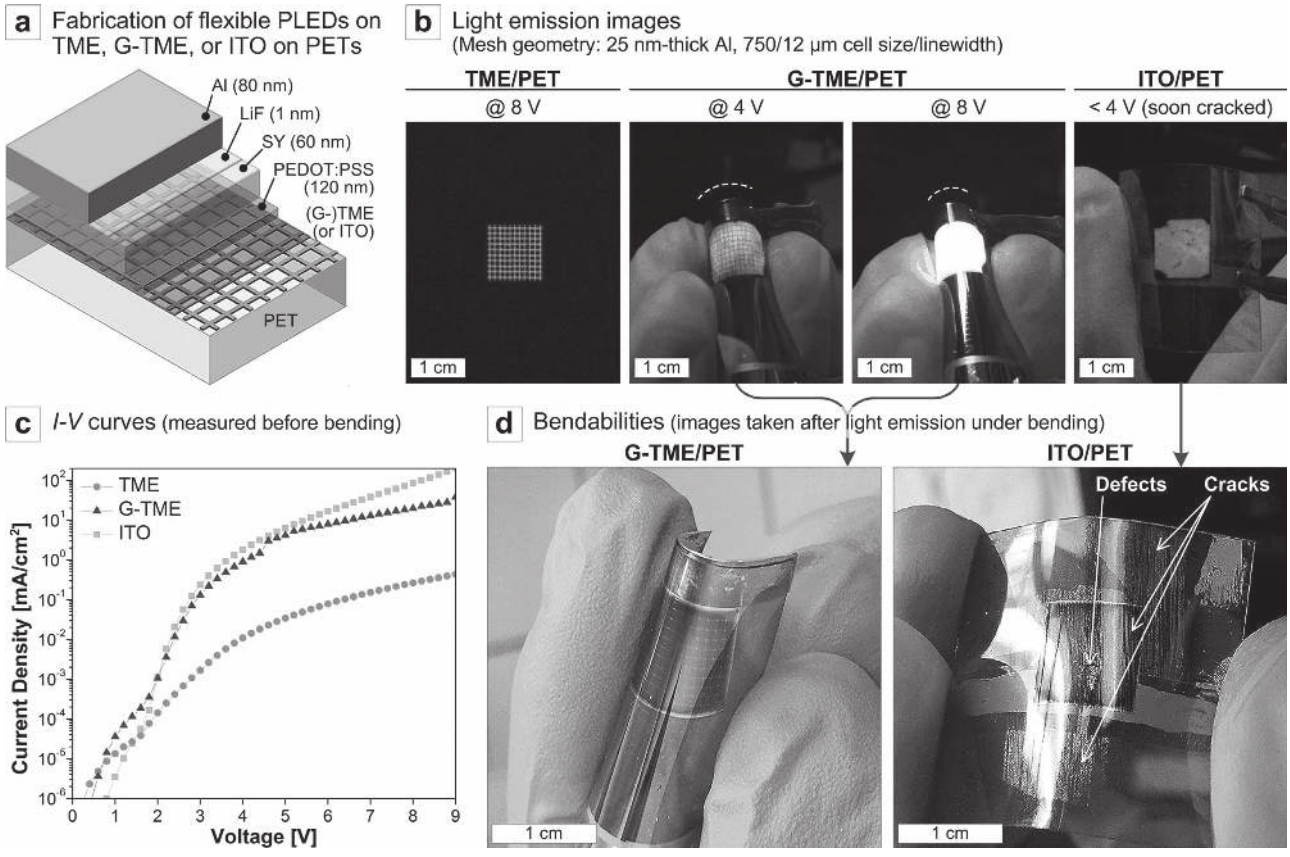

Figure 5. Fabrication of flexible PLED devices using (G-)TME or ITO formed on PET substrates as transparent electrodes: a) Device schematics where (G-)TME or ITO serves as an anode. b) Light-emission images under bending. The G-TME PLED device achieves stable luminance under bending while the ITO PLED device cracked right after the image was taken. c) *I–V* curves measured in unbent conditions. d) Close views of the flexible PLED devices after light emission tests under bending. The G-TME electrode appears intact while the ITO layer was severely damaged by cracks and defects.

G-TME compared to ITO. The current density and maximum luminance values of the G-TME are slightly smaller than those of the ITO PLED (Figure 5c) since the coarse TME with thin Al metal used in our PLED fabrication has a higher sheet resistance, yet these values can be improved by further optimizing the TME structure. Notably the graphene incorporated with TME functions as an effective current-spreading layer,[18] thereby resulting in much more uniform luminance over the entire electrode area (Figure 5b). As a result of the current spreading by the graphene across mesh openings, the current density can also be enhanced as compared to the TME without graphene (Figure 5c). Figure 5d confirms the durability of flexible (G-)TMEs; the G-TME appears clean and intact after light-emitting operations under repeated bending while ITO cracks after the first few bending cycles. This result is consistent with our previous study showing the constant sheet resistance of metal mesh pattern regardless of the bending angles, whereas the bent ITO quickly loses conductivity due to cracking.[11] Therefore PRL may find its specific competitiveness in flexible and large-area TME fabrication.

In summary, a new micro/nanofabrication methodology termed photo–roll photolithography (PRL) has been developed to realize continuous and scalable patterning by combining the outstanding advantages of photolithography and roll processing. Beyond pattern replication, PRL enables the geometry-tunable patterning by real-time modulation of relative mask–substrate motion. The gentleness of the PRL process further allows the use of delicate nanomaterials such as graphene as a substrate. We demonstrate the versatility and practicability of PRL which can be used for the continuous fabrication of various flexible optoelectronic products ranging from band-tunable IR filters to TMEs and PLEDs. PRL may potentially provide a solution for broader manufacturing needs which demand high-throughput micro/nanopatterning over large-area flexible substrates, toward next-generation electronics such as rollable touch screens and flexible displays.

Experimental Section

Setup and Operation of the PRL System: Overall, the PRL system consists of a photomask-attached rollable UV exposure unit, a linear-motorized substrate feeding system, and the developing module. First, a collimated UV source core was prepared by housing the 1 mm-wide slit over the UV lamp (CS 2010, Thorlabs, Inc.). This UV core was suspended inside a 90 mm-diameter hollow quartz cylinder with the slit facing downward, supported by ball bearings at both ends of a cylinder to allow the cylinder to rotate with a static UV core inside. A thin layer of PDMS (Sylgard 184, Dow Corning Corp.) was wrapped around the outer cylinder surface, and then a flexible photomask (see below for fabrication details) was conformally attached onto the PDMS pad. This rollable UV exposure unit was then arranged over a 3-DOF stage motorized by a linear piezo motor (CMA-12CC, Newport Corp.). The substrates were prepared and coated with photoresist for desired the fabrications (e.g., TMEs, graphene, and IR filters) as described in detail in the following section. The photoresist-coated substrate sample was then located on a motorized linear stage and was brought into contact (for identical patterning, e.g., TME fabrication) or proximity (for geometry-controlled patterning, e.g., IR filter fabrication) by controlling the stage axes so that the contact line between the substrate surface and the rolled mask was aligned to the UV exposing slit inside. As the mask rolling and substrate feeding proceed either isokinetically (in contact mode) or by independent controlling (in proximity) with the UV light on, a continuous UV exposure was conducted onto the sample through the photomask pattern. With the peak UV wavelength fixed at 365 nm, the intensity was regulated in the range of 40–200 mJ cm^{-2} depending on the pattern dimensions and processing speeds, to ensure consistent UV exposure. Finally, the sample passed through the developer bath (MF-319, Shipley) for about 1 min, finalized by the following metal etching which can be done in case of Al used in this study by an additional 1–2 min immersion in the developer.

Fabrication of a Flexible Photomask: First, original pattern masks were prepared on either a 5-inch Cr/glass mask plate by using a mask maker (for TME and IR filter patterns) or on a PET film by directly laser-printing the black and white image (shown in Figure 1c). Using this original mask, a flexible photomask was fabricated through the conventional photolithography process. A 50 nm-thick Al was first deposited on a PET film by using an e-beam evaporator (Enerjet Evaporator, Denton Vacuum, Inc.), followed by the spin-coating of a photoresist layer (S1815, Shipley) at 3000 rpm for 30 s. After soft-baking at 95 °C for 1 min, UV exposure was carried out through the prepared hard mask plate containing the desired patterns in a Karl Suss MA6 aligner for larger feature sizes (>1.5 μm) or a stepper (GCA AS200 AutoStep) for small features (ca. 500 nm). The sample with UV-exposed mask pattern was then developed in MIF-319 developer, accompanied by the additional 1–2 min immersion to etch the exposed Al layer as well. The residual photoresist layer was removed by acetone and cleaned by using isopropyl alcohol (IPA) to complete the fabrication of a flexible Al/PET photomask.

Preparation of Substrates: For IR filter samples, an MIM stack of Al (100 nm)–SiO_2 (200 nm)–Al (200 nm) was sequentially sputtered onto a PET sheet (Melinex 454, Tekra Corp.) by using a Lab 18–2 sputter tool (Kurt J. Lesker). For the Al mesh TME samples, the substrates were prepared by depositing 20, 30, or 50 nm-thick Al layers on bare or graphene-transferred glass pieces or PET sheets via e-beam evaporation (Enerjet Evaporator, Denton Vacuum, Inc.). See the next section for detailed graphene-transfer procedure. A thin layer of photoresist (Microposit S1805, Shipley) was spin-coated on these substrates, typically at 4000 rpm for 30 s followed by a 1 min bake at 95 °C.

Transfer of Graphene onto the Target Substrates: To transfer graphene from Cu to our target substrates, we used a technique similar to one described previously.[19] A graphene film grown on a Cu foil (Gratom M, Bluestone Global Tech.) was first spin-cast with a thin layer of poly(methyl methacrylate; PMMA, 950 A9, MicroChem Corp.) at 1750 rpm for 45 s, and naturally dried in the ambient environment. Then, the PMMA-coated graphene/Cu piece was floated on a $FeCl_3$ solution (Dalpro E-1G) to etch the Cu foil. Once all Cu was etched away (ca. 1.5 hours) the PMMA-coated graphene was scooped from the etchant bath with a clean glass cover-slip, followed by ample deionized (DI) water rinsing, and was floated in a DI water bath. The target transparent substrates, pretreated with O_2 plasma (55 sccm O_2, 160 mTorr, 150 W, 30 sec; Glen 1000-P Asher), were used to scoop the PMMA/graphene stack from the DI water bath. After completely drying under moderate (ca. 100 Torr) vacuum overnight, the PMMA layer was carefully removed by ample washing in acetone, IPA, and DI water, to leave only the graphene layer on the target substrate.

Characterization: SEM imaging was performed using a Philips XL30-FEG SEM, typically at the operating voltage of 10–25 kV after sputtering a thin Au film (<5 nm) to avoid electron charging if necessary. The IR reflection spectra of IR filter samples were measured by FTIR spectroscopy (Spectrum GX, Perkin-Elmer) with incident IR wavenumbers swept from 4000 to 400 cm^{-1} through a high-quality IR polarizer (KRS-5, Perkin-Elmer). The sheet resistances of fabricated (G-)TMEs were measured using a multimeter (GDT-311, Gardner Bender) after 100 nm-thick Al electrodes were additionally deposited at both ends of the (G-)TME sample after separating from nonpatterned surrounding area. For each sample, the distance between electrodes was varied to three different values to obtain the exact sheet resistance by extracting contact resistances originating between multimeter tips and sample electrodes. The optical transmittance measurements of (G-)TMEs were conducted using a Nikon Eclipse TE300 microscope

with a HR4000CG spectrometer (Ocean Optics Inc.). The *I–V* curve measurement of fabricated PLED devices was performed using a Keithley 2400 oscilloscope.

Acknowledgements

This work was supported by the National Science Foundation DMR 1120187 and CMMI programs.

Received: July 28, 2013
Published online: September 8, 2013

[1] M. J. Madou, *Fundamentals of Microfabrication and Nanotechnology*, Third Edition, Taylor and Francis, Boca Raton, FL, USA **2009**.
[2] a) D. Bratton, D. Yang, J. Y. Dai, C. K. Ober, *Polym. Adv. Technol.* **2006**, *17*, 94; b) L. J. Guo, *Adv. Mater.* **2007**, *19*, 495; c) Z. H. Nie, E. Kumacheva, *Nat. Mater.* **2008**, *7*, 277.
[3] P. Maury, D. Turkenburg, N. Stroeks, P. Giesen, I. Barbu, E. Meinders, A. van Bremen, N. Iosad, R. van der Werf, H. Onvlee, *Microelectron. Eng.* **2011**, *88*, 2052.
[4] J. G. Ok, H. S. Youn, M. K. Kwak, K. T. Lee, Y. J. Shin, L. J. Guo, A. Greenwald, Y. S. Liu, *Appl. Phys. Lett.* **2012**, *101*, 223102.
[5] a) S. H. Ahn, L. J. Guo, *Adv. Mater.* **2008**, *20*, 2044; b) S. H. Ahn, L. J. Guo, *ACS Nano* **2009**, *3*, 2304.
[6] J. A. Rogers, K. E. Paul, R. J. Jackman, G. M. Whitesides, *Appl. Phys. Lett.* **1997**, *70*, 2658.
[7] M. K. Kwak, J. G. Ok, J. Y. Lee, L. J. Guo, *Nanotechnology* **2012**, *23*, 344008.
[8] K. Ellmer, *Nat. Photonics* **2012**, *6*, 808.
[9] T. Xu, H. F. Shi, Y. K. Wu, A. F. Kaplan, J. G. Ok, L. J. Guo, *Small* **2011**, *7*, 3128.
[10] a) M. G. Kang, L. J. Guo, *Adv. Mater.* **2007**, *19*, 1391; b) M. G. Kang, M. S. Kim, J. S. Kim, L. J. Guo, *Adv. Mater.* **2008**, *20*, 4408.
[11] M. G. Kang, H. J. Park, S. H. Ahn, L. J. Guo, *Sol. Energy Mater. Sol. Cells* **2010**, *94*, 1179.
[12] M. G. Kang, H. J. Park, S. H. Ahn, T. Xu, L. J. Guo, *IEEE J. Sel. Top. Quantum Electron.* **2010**, *16*, 1807.
[13] S. Garaj, W. Hubbard, A. Reina, J. Kong, D. Branton, J. A. Golovchenko, *Nature* **2010**, *467*, 190.
[14] a) S. Lee, K. Lee, C. H. Liu, Z. H. Zhong, *Nanoscale* **2012**, *4*, 639; b) X. Li, Y. Zhu, W. Cai, M. Borysiak, B. Han, D. Chen, R. D. Piner, L. Colombo, R. S. Ruoff, *Nano Lett.* **2009**, *9*, 4359.
[15] Y. Zhu, Z. Z. Sun, Z. Yan, Z. Jin, J. M. Tour, *ACS Nano* **2011**, *5*, 6472.
[16] H. Youn, K. Jeon, S. Shin, M. Yang, *Org. Electron.* **2012**, *13*, 1470.
[17] T. H. Han, Y. Lee, M. R. Choi, S. H. Woo, S. H. Bae, B. H. Hong, J. H. Ahn, T. W. Lee, *Nat. Photonics* **2012**, *6*, 105.
[18] J. M. Lee, J. Yi, W. W. Lee, H. Y. Jeong, T. Jung, Y. Kim, W. I. Park, *Appl. Phys. Lett.* **2012**, *100*, 061107.
[19] a) A. Reina, H. B. Son, L. Y. Jiao, B. Fan, M. S. Dresselhaus, Z. F. Liu, J. Kong, *J. Phys. Chem. C* **2008**, *112*, 17741; b) X. S. Li, W. W. Cai, J. H. An, S. Kim, J. Nah, D. X. Yang, R. Piner, A. Velamakanni, I. Jung, E. Tutuc, S. K. Banerjee, L. Colombo, R. S. Ruoff, *Science* **2009**, *324*, 1312.